Study of a phosphorescent cationic iridium(III) complex displaying blue shift in crystals

Emiliano Martınez-Vollbert, Christian Philouze, Isabelle Gautier-Luneau, Yohann Moreau, Pierre-Henri Lanoë, Frédérique Loiseau

PCCP
Physical Chemistry Chemical Physics

Accepted Manuscript

This article can be cited before page numbers have been issued, to do this please use: E. Martínez-Vollbert, C. Philouze, I. Gautier-Luneau, Y. Moreau, P. Lanoë and F. Loiseau, *Phys. Chem. Chem. Phys.*, 2021, DOI: 10.1039/D1CP03341G.

ROYAL SOCIETY OF CHEMISTRY

rsc.li/pccp

View Article Online
DOI: 10.1039/D1CP03341G

ARTICLE

Study of a phosphorescent cationic iridium(III) complex displaying blue shift in crystals

Received 00th January 20xx,
Accepted 00th January 20xx

DOI: 10.1039/x0xx00000x

Emiliano Martínez-Vollbert,[a] Christian Philouze,[a] Isabelle Gautier-Luneau,[b] Yohann Moreau,[c] Pierre-Henri Lanoë,[a]* and Frédérique Loiseau[a]*

Abstract: We report the synthesis and the characterization of a new cationic iridium(III) complex featuring two 1-(p-methoxyphenyl)-5-methoxybenzimidazole cyclometallating ligands and a dimethylbipyridine ancillary ligand. The complex has been fully characterized by 1D and 2D NMR (^{1}H, ^{13}C, ^{19}F and ^{31}P), elemental analysis and high-resolution mass spectrometry (HRMS). The photoluminescence studies performed in solution, on amorphous powder and on crystals revealed an unexpected behavior. Indeed, the emission spectra displayed in both solution (CH_2Cl_2) and amorphous powder samples are centered around 580 nm, whereas in crystals the emission displays a large hypsochromic shift of ~800 cm^{-1} (λ_{em} = 558 nm). X-ray diffraction experiments, photophysical studies and DFT calculation allow to rationalize the hypsochromic shift.

Introduction

Phosphorescent iridium(III) complexes know an intensive research since the beginning of the 21st century for a large number of applications such as emissive material in optoelectronics, photosensitizers and dyes for biological imaging to name a few. [1–6] Iridium(III) complexes offer many advantages such as high quantum efficiency, electrochemical stability and reversibility, accessibility by reliable and robust methods and tuneable colour of emission, that spans from sky blue to near-infrared.[7] Thanks to the important spin-orbit coupling due to the presence of the heavy metal, all the molecules in the singlet excited state undergo nearly quantitatively an intersystem crossing to the triplet excited state. The emission of iridium(III) complexes emanates often from the radiative deactivation of metal-to-ligand triplet excited state (^{3}MLCT*) to the ground state. In many cases the luminescence is ascribed to the radiative deactivation of mixed triplet MLCT/LC excited states (LC: ligand centered). [7,8] Discrimination of the emission origin is accessible by the steady state and time resolved emission spectroscopy investigation, as well as with the help of calculation.[9]

Many applications need high emission quantum yield in the solid state, such as Organic Light-Emitting Device (OLED) and Light Emitting electrochemical Cells (LEECs). Unfortunately, the luminescence of chromophores, and particularly cyclometallated iridium(III) complexes, in neat solid is subject to dramatic quenching and the phenomenon is referred to "aggregation-caused-quenching".[10] For example, [Ir(ppy)$_3$] displays photoluminescence quantum efficiency of 0.97[11] in dilute solution, whereas in neat film the value drops below 0.03[12] and as an amorphous solid the complex is almost non luminescent.[13] The drop of quantum efficiency from solution to solid has been assigned to self-quenching through intermolecular π-stacking interactions and triplet-triplet annihilation.[6,14] The introduction of bulky groups, such as dimethylphenyl, mesityl, phenyl or *t*-butyl, to name a few, on the ligands framework[15–18] and "shielding" of the metal center by macrocyclic ligands[14,19] allow inhibiting these interactions. For example, the iridium(III) complex from reference[20], represented in figure 1 featuring the bulky 4,4'-di-tert-butyl-2,2'-bipyridine ligand, has unchanged photoluminescence efficiency from solution to the spin-coated film, with QY of 68% in deaerated CH_3CN and 72% in film. In contradiction, some other complexes display low or almost no luminescence in solution and the "turning on" of the luminescence is triggered by aggregation either by the introduction of a non-solvent or in the solid state (powder, neat spin-coated film or drop casted film…). This behaviour has been called in different manner "enhanced phosphorescence emission in the solid state" (EPESS) and "aggregation-induced phosphorescent emission" (AIPE)[6,21–23], depending if the complex displays in dilute solution a weak emission or no detectable emission, respectively. In all these cases, the complexes skeleton demonstrates flexibility in solution, and thus the excitation energy is dispersed thermally. In the solid or aggregated state, the stiffening of the structure leads to "turning on" of emission.

[a] Univ. Grenoble Alpes, CNRS, DCM, 38000 Grenoble, France. E-mails : pierre-henri.lanoe@univ-grenoble-alpes.fr and Frederique.loiseau@univ-grenoble-alpes.fr
[b] Univ. Grenoble Alpes, CNRS, Grenoble INP, Institut Néel, 38000 Grenoble, France
[c] Univ. Grenoble Alpes, CEA, CNRS, IRIG, CBM, F-38000 Grenoble, France

Electronic Supplementary Information (ESI) available: [details of any supplementary information available should be included here]. See DOI: 10.1039/x0xx00000x

View Article Online
DOI: 10.1039/D1CP03416C

Figure 1. 4,4′-di-tert-butyl-2,2′-dipyridyl-bis[2-(2′,4′-difluorophenyl)pyridine]iridium(III) isolated with hexafluorophosphate anion from reference.[20]

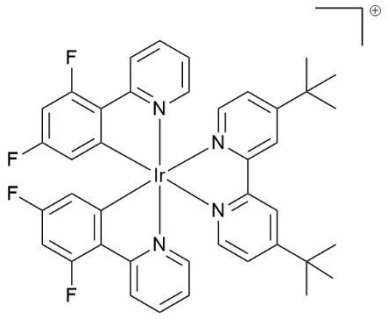

Changes in the emission wavelength in the solid state is quite common especially looking at the neat solid (powder, neat thin film and crystal). The large majority of the cationic iridium(III) complexes display a bathochromic shift in solid state,[17,23,32–34,24–31] whereas only few contributions report iridium(III) complexes displaying a hypsochromic shift.[17,27,40,32–39] If bathochromic shifts could be easily rationalized with the presence of intermolecular interactions, such as π-π interactions, [14] blue shifted emission spectra in solid state are less straightforward dealing with neat solid. In addition, the understanding of solid-state emission deals mainly with compounds displaying mechanochromism or piezochromism, which is the property of certain materials to change color by the application of pressure, usually through grinding.[41] For example, the cationic Ir(III) complex with 2-phenylpyridine as cyclometallating ligands and the 2-(5-phenyl-2-phenyl-1,2,4-triazol-3-yl)pyridine ancillary ligand (Figure 2) displays blue shift emission in solid state, as well as mechanochromism.[40] The "as synthesized" powder displays an emission centered at 471 nm, whereas the emission in diluted CH_3CN solution is centered at 499 nm. When grinding the "as synthesized" powder the emission displays a bathochromic shift and is similar to the emission observed in solution. Such a behavior was ascribed to phase transition from polycrystalline powder assessed by powder X-ray diffraction (PXRD) to amorphous phase. Nevertheless, the reason of the blue shift in crystalline state was not stated.

Figure 2. Ir(III) complex with phenylpyridine as cyclometallating ligands and the 2-(5-phenyl-2-phenyl-1,2,4-triazol-3-yl)pyridine isolated with PF_6 anion, from ref [40].

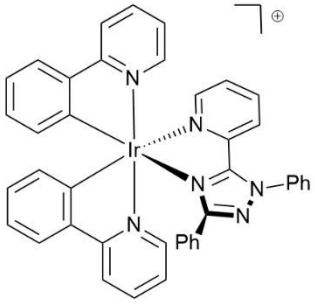

Most of the cationic iridium complexes studied for lighting application are derived from the archetypical 2,2′-dipyridyl-bis[2′,4′-phenylpyridine]iridium(III) complex ($[(ppy)_2Irbpy]^+$, with ppy = 2′,4′-phenylpyridine and bpy = 2,2′-dipyridine), where the introduction of electrodonating or electron withdrawing groups over the ligand allows to tune efficiently the emission wavelength of the complex.[42–45] For example, the archetypical $[(ppy)_2Irbpy]^+$ displays an emission centered at 585 nm (QY = 14% in deaerated CH_3CN) [46], whereas the above mentioned complex with fluorine atoms (electron withdrawing effect) over the phenyl rings displays an emission centered at 512 nm (QY = 70% in CH_3CN).[20] On another hand, cationic complexes featuring 2-phenylbenzimidazole cyclometallating ligands are less common.[29,36,47–51] This ligand presents as advantages to give several divergence points (i) the benzimidazole ring (phbnz), (ii) phenyl ring and (iii) the substitution of the nitrogen atom in position 3 (*Figure 3*) and its synthesis does not require the use of palladium-catalyzed cross-coupling reactions.[52,53] The three positions could give access to a fine tuning of the emission properties and modification of the *bulkiness* of the final complex. In this contribution, we present a study of complex **A** with methoxy groups both in position 4 of the phenyl ring and position 5 of the benzimidazole moiety. The investigation of the photoluminescence properties in solution and solid samples (measured on crystals and on amorphous powder) revealed a hypsochromic shift in the crystal state. This behavior has been correlated with the organization of complex **A** in the crystals. Furthermore, crystal structure of complex **A** has been determined, and PXRD has been measured.

Figure 3. Left, general structure of cationic iridium complexes featuring 2-phenylbenzimidazole cyclometallating ligand. Right, complex **A** presented in the contribution.

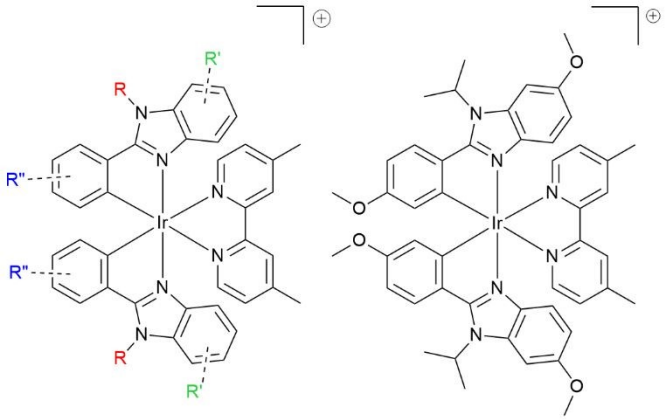

Methods

Synthesis of complex A

Complex A has been synthesized following a two steps procedure (Scheme 1) well described in the literature,[17] that involved the formation of dimer $[(C^N)_2Ir(\mu\text{-}Cl)]_2$ by the methods described by Watts *et al.*[54] and, in a second step, the introduction of the dimethylbipyridine (dmp) ligand. Complex **A** has been isolated after chromatographic column followed by a rapid precipitation of the desired fraction with an overall yield of 67%, and characterized by NMR (^1H, ^{13}C, ^{19}F and ^{31}P), HRMS

DOI: 10.1039/D1CP03741C

and elemental analysis. More details about the synthesis procedure and characterisation are available in the Electronic Supporting information (ESI).

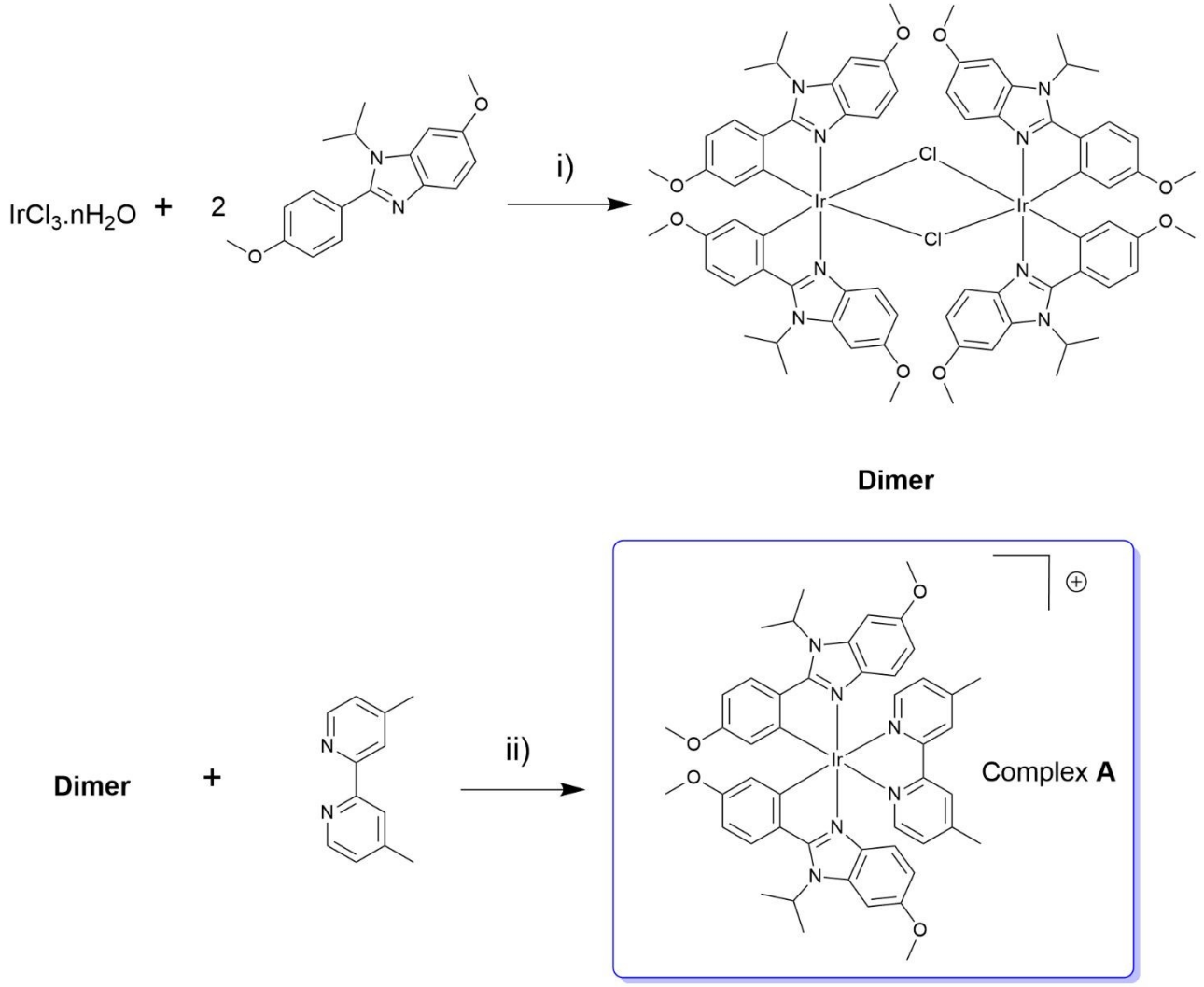

Scheme 1: Synthesis of complex A, i) H2O/EtOEtOH (1/3), refluxed overnight; ii) MeOH/CH2Cl2 (1/1) refluxed overnight under Ar, then KPF6 (sat.).

Preparation of the solid samples

The amorphous powder (referred as powder hereafter) was obtained by rapid precipitation of the material obtained after chromatography column by adding pentane in a concentrated solution of the complex in dichloromethane followed by filtration over Millipore® apparatus.

The crystals were obtained by slow vapor diffusion of diisopropylether in a concentrate solution in 1,2-dichloroethane. The process was repeatable and gave in each case dark orange crystals displaying green-yellow emission under UV-light. The resulting solids were collected indiscriminately and used for the emission spectroscopy experiments and for the PXRD measurements.

Structural Study

Crystal Structure Determinations and Refinements. The crystals display orange colour under daylight as the amorphous powder, but display a yellow emission under UV-light which differs from the orangey emission of the amorphous powder. The compound ($[C_{48}H_{50}IrN_6O_4](PF_6)\cdot 3C_2H_4Cl_2$) crystallizes in monoclinic C2/c space group with the cell parameters: a = 19.554(4) Å, b = 22.055(4) Å, c = 15.394(3) Å and β = 117.07(3) °, V = 5911(2) Å^3, Z'=4. A yellowish plate crystal (0.13 x 0.15 x 0.30 mm) was picked up, coated with a paraffin mixture and mounted with a nylon loop and centered on a Bruker-Nonius diffractometer equipped with an Incoatec high brilliance microsource with multilayers mirrors monochromatized Mo(Kα) radiation (λ = 0.71073 Å) and an APEX II detector. Data were collected at 200 K with an Oxford Cryosystem to avoid the deterioration of the crystal, that displays fragility when manipulated. Final cell parameters were obtained post-refining the whole data. The collected reflections were corrected for Lorentz and polarization effects (EVAL14) and for absorption (SADABS). The resulting data were merged using XPREP. Using

View Article Online
DOI: 10.1039/D1CP03341G

the OLEX 2 analysis package, the crystal structural solution was solved by charge flipping method (Superflip) and refinement was done by full-matrix least squares on F2 (SHELX2013). All non-hydrogen atoms were refined anisotropically. H atoms were set geometrically, riding on the carrier atoms, with isotropic thermal parameters. PF_6 anion and dichloroethane molecules displayed disorders which were treated using different positions with partial occupancy rates and restraints. The crystallographic details, selected bond lengths and angles are given in Tables S1 and 1 respectively. CCDC number 1981001.

Powder X-ray diffraction details

Powder X-ray diffraction (PXRD) was assessed under ambient conditions using a Siemens D8 Advance diffractometer (Cu Kα radiation, 40 mA, 40 kV) in the 3−60° 2θ range with a 0.01°step size and an acquisition time of 6 s/step.

Photophysical characterisation

The UV-visible spectra have been performed on a Varian Carry 300 using 1 cm path quartz cells. Steady state photoluminescence measurements of the liquid sample were carried out on a Horiba Fluoromax 4 using four walls quartz cuvettes with 1 cm path and samples were degassed using the "freeze-pump-thaw" technique and for solid samples (crystals and powder) the spectra were acquired with a Horiba Fluorolog equipped with a "front face" acquisition set. The photoluminescence quantum yields (PLQY) were determined using $Ir(ppy)_3$ in dichloromethane as reference for liquid samples and PLQY solid samples were determined using a GMP G8 integrating sphere fitted in a fluorolog. Time resolved photoluminescence measurements of liquid sample were performed on a Edinburgh Instruments nanosecond transient absorption LP920 equipped with a pump laser Quantel Brilliant emitting at 355 nm.

DFT and DFT:MM calculations

All the DFT and DFT:MM calculations were carried out with the Gaussian 16 program,[55] using the multilayer ONIOM method[56] for the DFT:MM approach. The MN15[57] density functional was used with the double-zeta Def2SVP[58,59] basis set for all atoms (which includes an effective core potential for Ir(III) for the QM part, while the UFF[60] forcefield was used to describe MM atoms, using (and checking) the automatic assignment by the gaussian program. All ONIOM calculations were done with the "embed" keyword, in order to include the field of charges during the DFT SCF procedure, thus accounting directly for polarization of the wave function. The model of the crystal was built by creating a 7*7*7 supercell starting from experimental positions using Mercury[61] and ambertools.[62] The central complex molecule was then selected and only molecules and counterions with at least one atom within a distance lower or equal to 25 Å from the selected molecule were kept. To ensure that the selection was electrically neutral, the same number of complexes and counterions (162 of each) was kept in the structure around the molecule of interest, representing a total of 18792 atoms: see Figure 4.

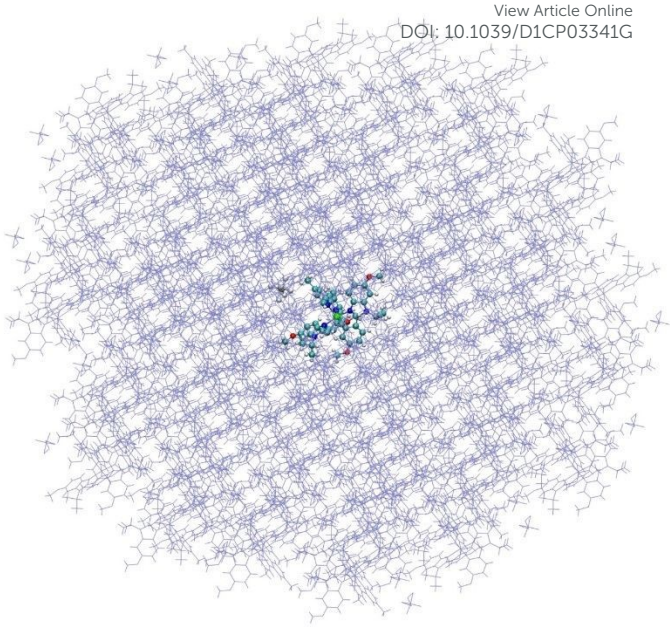

Figure 4: Molecule and counterion embedded in a crystal part including all molecules with a part at a distance lower or equal to 25 Å from the molecule.

This model has first been used to determine the charges of the surrounding MM layer. For that, we have used an approach similar to the one described by Bjornsson *et al.* [63] In a first step, electrostatic charges were defined for the isolated molecule+PF_6^- system in their crystal geometry, using DFT. The chelp [64,65] and MK [66] ESP fitting methods were used. The charges obtained with these two methods differ notably from each other: for instance, only the chelp method give the Ir cation a positive charge. Nevertheless, very similar results were found for both, and only results obtained with the chelp set of charges are shown in the present work. The set of charges thus determined has been attributed to corresponding atoms in all molecules of the crystal model. A new set of charges, determined on the central QM complex + counterion was determined within the field of charges created by the MM surroundings, and attributed to all the molecules. This procedure has been conducted iteratively for 50 steps. A rapid convergence (c.a. 10 steps) to the 3rd digit was found and final atomic charges were taken as the average over the 20 last steps. Once the charges of the surroundings determined, the model could be used to determine luminescence properties.

In this new step, the PF_6^- counterion, initially in the QM part for the determination of electrostatic charges was put in the MM part (hence keeping its crystallographic position) with the charges computed in the previous step; the charge of phosphorus atom in this sole counterion (but not the surrounding ones) was adjusted to keep a neutral molecule and a total charge of -1 for the MM part and +1 for the central Ir complex.

The geometry of the central complex was optimized in its triplet state, all the MM atoms being kept frozen, thus accounting for both mechanical and electronic embedding.

View Article Online
DOI: 10.1039/D1CP03341G

We have considered that the emission process could be described as a vertical (adiabatic) transition, *i.e.* without change of geometry along the de-excitation process. Therefore, the energy of the complex in its singlet state, with the optimized geometry of the triplet state, has also been determined. The transition energy, noted $\Delta E_{T\rightarrow S}$, is determined as the energy difference between the two states and also used to compute the wavelength of the emitted photon during the vertical transition.

To compare properties of the Ir complex in crystal to the one in solvent or powder, a similar calculation was done on the isolated complex: geometry optimization in the triplet state and single point calculation on the same geometry in singlet state followed by the evaluation of the energy difference.

Results and discussions

Crystal structure

The iridium(III) and the P atom of the $([IrL_2(dmp)](PF_6)\cdot 3C_2H_4Cl_2)$ compound are lying on a 2 fold axis. The asymmetrical unit is constituted of a half Ir atom, a half dimethylbipyridine (dmp), one L ligand, a half PF_6 anion and one and half solvent molecules. The packing is represented along the three axes in figure S1 and S2, in which it can be seen that cation chains (*vide infra*) are separated by the hexafluorophosphate anions. The complex displays a distorted octahedral geometry (Figure 5 and Table 1). The angles formed by the nitrogen atoms from the cyclometallating ligands and the nitrogen atoms from the dmp are ~99.4 ° and ~87.4 °, respectively. Only the angle between the cyclometallating carbons around the Ir is almost ideal (~90,2 °). Distorted octahedral geometry is commonly observed in cyclometallated cationic iridium complexes,[15,31,37,46,67–70] and it is also observed in the commonly called archetype complex $[Ir(ppy)_2bpy]^+$.[46] The coordinating nitrogen atoms from the benzimidazoles are in the expected *trans* position[46] with each other (~171.4 °). As expected in centrosymmetric space group, the Δ and Λ isomers in alternance in the lattice and between two chains (Figure 5 and Figure 7) are observed and are formed during the cyclometallation step.[71] The bite angles of the ligands are ~77.5 ° (dmp) and ~79.3 ° (phbnz), the latter being very similar to the phenylpyridine ligand bite angle (~80 °).[46]

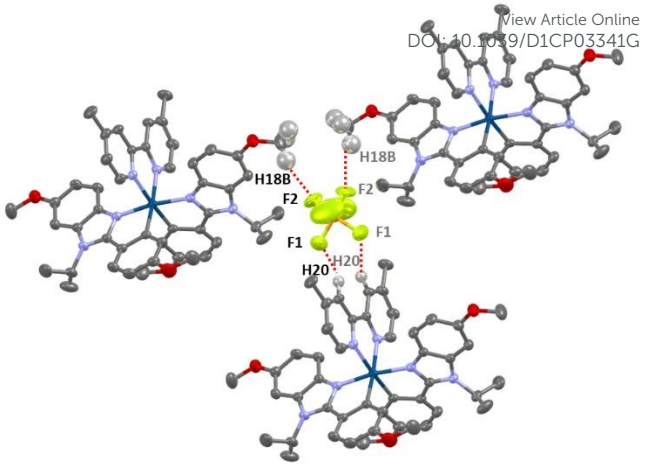

Figure 5. Representation of the Λ (left) and Δ (right) isomers of complex A with ellipsoid drawn at 50% probability showing the label scheme (symmetry card for grey labels (1-x, y, 3/2-z)); hydrogen atoms have been omitted for clarity.

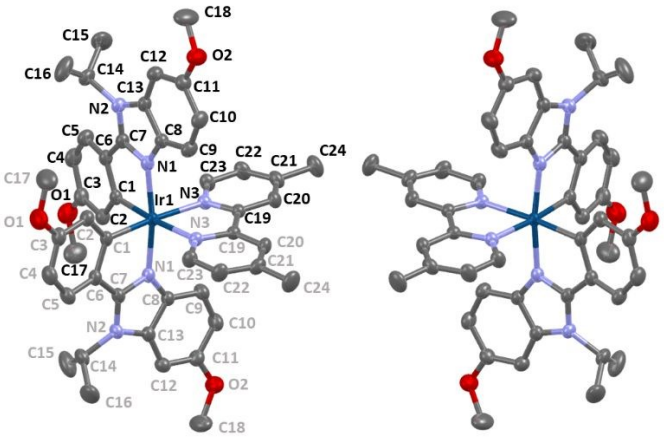

Figure 6. Representation of the hydrogen bonds linking the PF_6 anion and three cationic complexes **A**, hydrogen atoms involved are highlighted.

The bond lengths (Table 1) of the coordinating atoms with Ir are ~2.02 Å, ~2.04 Å, ~2.13 Å for the carbon atoms, the nitrogen atoms from the cyclometallating ligand and the nitrogen atoms from the dmp ligand, respectively. The bond lengths are very similar to those encountered in $[(ppy)_2Irbpy]^+$ with 2.01 Å, 2.05 Å and 2.13 Å, for Ir-C, Ir-N and Ir-N_{bpy} respectively.[46] In addition, the Ir-N_{bpy} bonds are longer due to the so called *trans* effect in agreement with the strong σ-donating ability of the carbon atoms.[46] The dmp ligand is almost planar with a deviation of roughly 3.7 ° between the two average plans of the pyridine rings, whereas the cyclometallating ligands deviate significantly with an angle of roughly 12 ° between the average plans of the phenyl and of the benzimidazole moieties. The cyclometallation induced an obvious rigidification of the phenylbenzimidazole ligands that restricts the motion of the *iso*-propyl groups. Indeed, no disorder is observed for these groups. The H5···*H14*C$(CH_3)_2$ distance is 1.973 Å, which is below the sum of the van der Waals radii (2.18 Å). These interactions could be the origin of the important angles between the phenyl and the benzimidazoles rings.

View Article Online
DOI: 10.1039/D1CP03344C

The complexes in the lattice are organized in chains and the PF_6 anions, as well as solvent molecules ($ClCH_2CH_2Cl$), fill the space between them. Along the b axis, one can observe an alternation in the orientation between two adjacent molecules, as well as in the chains (**Figure 7** and Figure S3-4). The complexes display intermolecular interactions and are organized in a somewhat catenary fashion along the ac direction. Within the chains, weak H···π interactions are found between the hydrogen atom H22 from the dpm ligand and the C12-C13 bond from the benzimidazole moiety (Figure S5). Counter ions deck chains through weak hydrogen bonding (**Figure 6**, **Table 2**). The interactions are displayed between the hydrogen atoms H20 of the dmp and fluorine atoms F1 from the counter ion and between the hydrogen atom H18B of OMe group on the

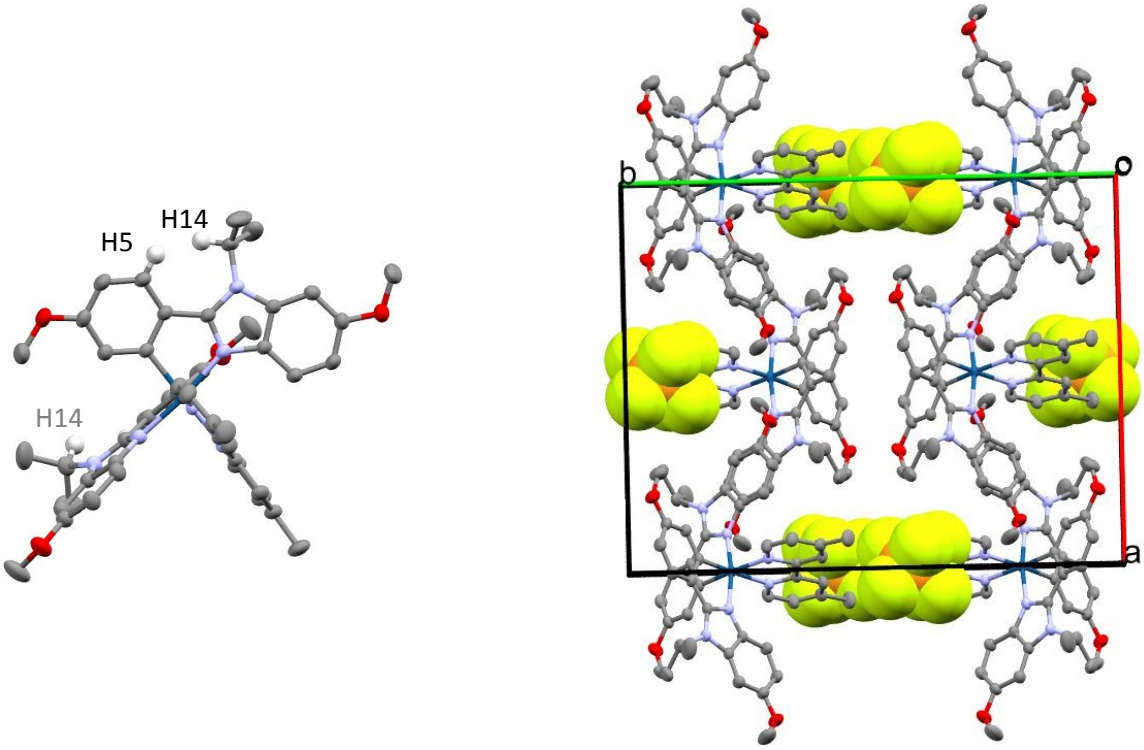

Figure 7. (Left) Crystal structure of complex **A** represented with ellipsoid drawn at 50% probability. H5 and H14 have been highlighted. (Right) Crystal packing projection in(a,b) plane, hydrogen atoms have been omitted for clarity, PF_6 anions are represented in space-fill, dichloroethane solvent have been omitted

benzimidazole moiety and the fluorine atoms F2.§ In addition, intramolecular hydrogen bonding is also observed between the H9 hydrogen atom riding by C9 carbon atom of the cyclometallating ligand and nitrogen atom N3 of the dmp ligand (Figure S6). The angles formed by the hydrogen atoms, carbon atoms, and acceptor atoms (XHA angles[72]) are over 135° and the X···A distances are in the range 3.6-3.8 Å. The intermolecular interactions could be ascribed to weak hydrogen bonding with an electrostatic nature. [72]

Table 1. Selected bond lengths and angles.

Ir1-C1 (Å)	Ir1-N1 (Å)	Ir- N3 (Å)	N_{C^N}^Ir^N_{C^N} (°)	C^N bite angle (°)	C_{C^N}^Ir^C_{C^N} (°)	dmp bite angle (°)
2.024(2)	2.037(2)	2.126(2)	171.38(11)	79.30 (9)	90.15(13)	77.47(11)

Table 2. Hydrogen bonds list.

Atoms (X, H, A)	X-H (Å)	H···A (Å)	X···A (Å)	H-X···A angles(°)
C20, H20, F1	0.95	2.49	3.378(4)	156.3
C9, H9, N3	0.95	2.63	3.369(4)	135
C18, H18, F2	0.98	2.49	3.362(15)	148.6
C22, H22, Centroid (C12-C13)	0.95	2.70	3.502	142.4

View Article Online
DOI: 10.1039/D1CP03741C

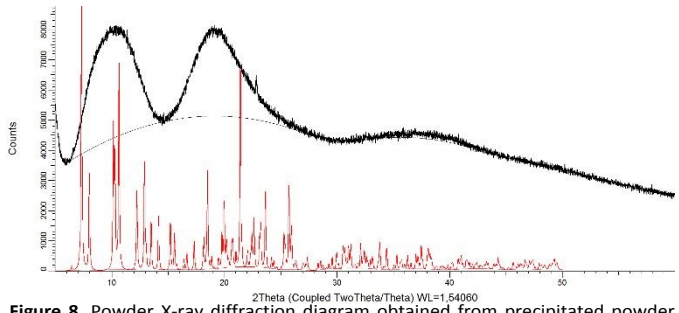

Figure 8. Powder X-ray diffraction diagram obtained from precipitated powder (black) and the calculated pattern from crystal structure (red).

Powder X-ray diffraction

The complex displays different colours in the powder and crystal forms, which may be related to polymorphism.[23,36,38,73–75] The powder XRD pattern displays three undefined humps roughly centered at 10 °, 19 ° and 37 °. The absence of fine peaks demonstrates that the precipitated powder is amorphous. It is worth noting that the present result differs from previous reports, where crystalline powders (PXRDs displayed sharp and intense diffraction peaks) were obtained with cationic iridium complexes either by evaporation of the solvents after chromatography column or by rapid recrystallization/precipitation.[23,36,39,40,74,76] In contrast, the crystals, collected indiscriminately from the same batch of crystallization, display a different pattern than the powder (Figure S8) with sharp peaks, which pattern is similar to the calculated one from the crystal structure.

Absorption and emission spectroscopies

The absorption and emission properties (steady state and time resolved) of the complex have been studied in both dichloromethane and acetonitrile under air equilibrated and deaerated condition, regarding the emission. The spectra are displayed in Figure 9 left and the quantum yields and lifetimes are gathered in Table 3.

The absorption spectrum displays in the UV region intense transitions, that can be ascribed to spin-allowed π-π* transition (^{1}IL) from the cyclometallating ligand and the ancillary ligand. Between 330 nm and 425 nm, moderately intense absorption bands are attributed to spin-allowed charge transfer transitions, from the metal to the ligand (^{1}MLCT) and from the cyclometallating ligand to the ancillary ligand (^{1}LLCT).[7] The tail observed above 420 nm is due to direct spin-forbidden transitions leading to ^{3}MLCT, permitted by the high spin-orbit coupling constant (ζ = 3909 cm^{-1}) of the iridium core.[7] Simulated spectrum, oscillator strength corresponding the absorption bands and orbitals involved can be found in ESI.

The complex displays a broad and unstructured orangy emission (Table 3 and Figure 10) with a PLQY of 13% and 4%, in CH_2Cl_2 and CH_3CN respectively. The emission of the complex is sensitive to the presence of molecular oxygen with a quenching constant (k_Q) of the order of 3.10^9 M^{-1}.s^{-1} in both solvents. §§ The time resolved spectroscopies revealed a long lived emission in the range of hundreds of ns, which is typical of phosphorescent cationic iridium(III) complexes emitting in this region of the spectrum [16,45,77]. The radiative deactivation constant k_r can be extracted from the emission data and it is of the order of 3.10^5 s^{-1}, which corresponds to a radiative process emanating from the deactivation of a triplet metal-to-ligand-charge-transfer excited state (^{3}MLCT*) to the ground state.[7,8] The latter is corroborated by the broadness of the emission and the positive solvatochromism (+510 cm^{-1}) of the emission,[7,8] when comparing the emission in CH_2Cl_2 and CH_3CN. Finally, complex **A** displays at 77 K in glassy butyronitrile a structured emission with two peaks at 527 nm and 557 nm with a very long decay (~18 µs). This rigidochromism is typical of transition metal complexes submitted to a rigidification of the environment by a decrease of the temperature (vide infra) and is mainly observed when the emission arises from the radiative deactivation of the ^{3}MLCT* to the ground state. Thus, the emission properties of complex **A**, emission shape, k_r, positive solvatochromism and rigidochromism, indicate that the phosphorescence has for origin the radiative deactivation from the ^{3}MLCT*, nonetheless cyclometallated iridium(III) complexes are known to display emission from the radiative deactivation of mixed excited state being mainly ^{3}MLCT*/^{3}LC*[7,8] and the emission might be best described as emanating from the radiative deactivation to the ground state of such mixed excited state with a predominance of the ^{3}MLCT* as confirm by the calculations (see ESI).

Figure 9. Top: Absorption and normalized emission spectra in CH_2Cl_2 (purple), in CH_3CN (green) and at 77 K in butyronitrile (yellow dotted line). Bottom: Normalized emission spectra from the powder (red) and the crystals (blue).

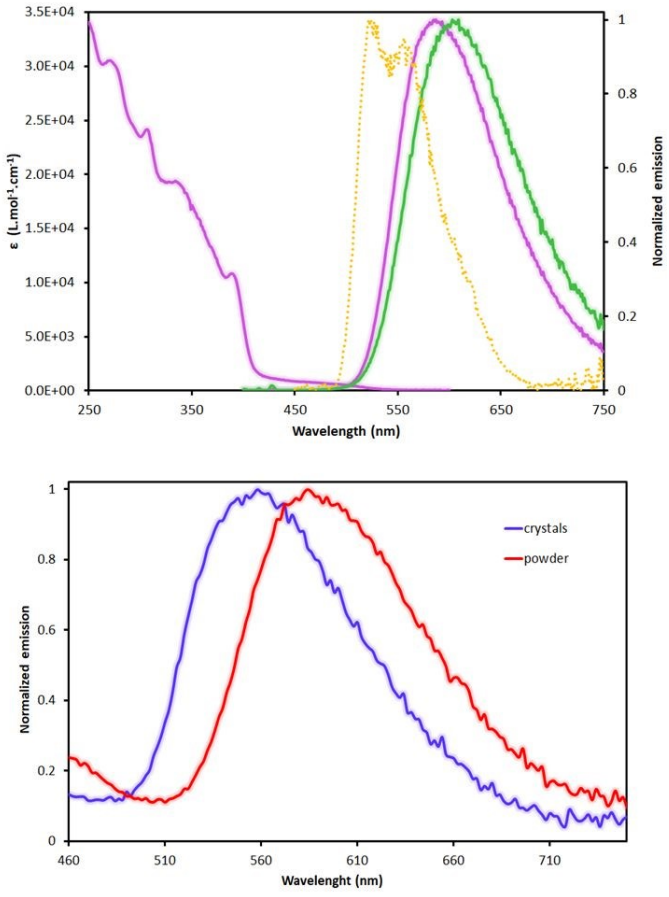

View Article Online
DOI: 10.1039/D1CP03341G

Table 3. Luminescence data for crystals and powder samples under air and at room temperature and in diluted deaerated solutions at room temperature.

	λ_{em}	Φ (x 10^{-2})	τ (ns)	Δ_{em}[1] (cm^{-1})	k_r x 10^5 (s^{-1})	k_{nr} x 10^5 (s^{-1})	$k_Q[O_2]$ x 10^9 ($M^{-1}.s^{-1}$)
Powder	585	5.4	1 580	0	-	-	-
Crystals	558	7.2	1 518	-798	-	-	-
CH_2Cl_2	585	13.0	570	-	3.0	20.0	3.5
CH_3CN	603	4.0	260	+510	3.6	93.0	2.9
77 K[2]	527[3], 557	n.d.	18 440				

[1] The shift in emission is determined taking the dichloromethane solution as reference, positive values refer to a bathochromic shift and *vice versa*. [2] In butyronitrile. [3] Most intense emission band. Experimental decay curves are given in figure S8

The solid-state emission has been explored in neat solid (i.e. amorphous powder and crystals), in steady state spectroscopy under air atmosphere. Photos of the crystals and the powder displayed in **Figure 10** allow to visualize at the naked eye the stark contrast of the emission of the amorphous phase and the crystal. Data are gathered in Table 3 and the spectra are displayed in Figure 9. The powder was obtained by precipitation of complex **A** from a dichloromethane solution with pentane. Both solid forms of the complex (i.e. powder and crystals) display a broad and structureless emission in the visible region of the spectrum which is an indication that the emission should emanate from the same radiative process (^{3}MLCT*/^{3}IL*) as in solution, which have been confirmed by the calculation (see ESI). Nevertheless, the emission spectrum of the powder is centered at 585 nm which is the same as the one observed in deaerated dichloromethane solution and in stark contrast the emission of the crystals displays a somewhat strong hypsochromic shift of 27 nm (798 cm^{-1}).

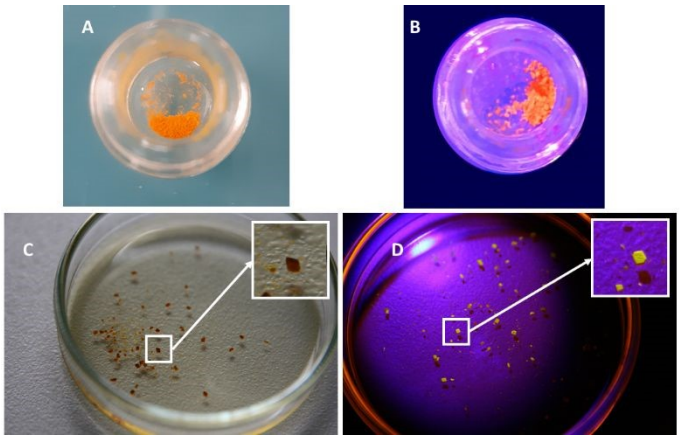

Figure 10: Photography of the complex under daylight (A,C) and UV-light at 265 nm (B,D). A and B show amorphous phase. C and D show isolated crystals. Dark dots correspond to the shadow of the crystals.

Such a shift solely in the crystal state is unusual (vide supra). This behaviour could be ascribed to rigidochromism which is a property of the transition metal complexes displaying a blue shifted emission when their solution environment becomes rigid, thus decreasing the stabilization of the emissive excited states, by lowering temperature [78] or increasing the pressure.[79] It is especially encountered with phosphorescence emanating from the radiative deactivation from the ^{3}MLCT* to the ground state. Nevertheless, rigidochromism has been ascribed to a tetranuclear $[Au_2Cu_2(\mu\text{-}(PPh_2)_2py)_2(\mu\text{-}OH)](PF_6)_3$ cluster with butterfly shaped metal core, that displays a very strong hypsochromic shift (172 nm, 4765 cm^{-1}) from CH_2Cl_2 solution to powder at room temperature.[80] This behaviour was attributed to the Jahn–Teller distortion in the lowest triplet excited state from linear to bent geometry around the gold(I) centers. Such an effect is unlikely to occur in octahedral d^6 iridium(III) cyclometallated complexes[81] and, in addition, the hypsochromic shift is observed solely in crystal for complex **A**, thus ruling out rigidochromism . Regarding the supramolecular organisation in the crystal, no evidence of the presence of strong intermolecular interactions is found, and especially no π-π stacking, that could lead to such hypsochromic shift. In addition, the intrinsic octahedral geometry of complex **A** prevents the formation of H-aggregates (or J-aggregates) both in solution and in solid state (crystal or powder).[82,83] An hypsochromic shift has been reported in a dinuclear rhenium(I) complex [84] and was ascribed to the local packing in the crystal and especially to the orientation of the molecular dipoles. In the case of complex **A**, a close look to the crystal lattice and especially to the projection in the ab plan (figure 5b) and the views displayed in Figure S1-4 show that the complexes, and, thus, the molecular dipoles, are oppositely oriented. Assuming that the excited state of the complex displays a higher molecular dipole moment than the ground state (in absolute value), it follows that the excited state could be destabilized. Consequently, the radiative deactivation of the excited state will be blue shifted in comparison with the solvated complexes. In addition, the crystal structure displays the presence of PF_6 anion close to the dmp ligand, highlighted by weak hydrogen bonds (*vide supra*). One can predict that the negative charge beared by the counter ion may interfere also with the dipole moment and thus it would destabilize the excited state leading to the observed hypsochromic shit in the crystal. Whereas, in the amorphous powder, the complexes are randomly oriented, as the PXRD shows and thus neither particular molecular dipole interaction or interactions with the counter ions are present. To have a deeper understanding of the phenomena and to discriminate if rather the dipole-dipole interaction or the peculiar position of counter ion lead to the hypsochromic shift we have performed DFT and DFT:MM calculations.

DFT and DFT:MM calculations

View Article Online
DOI: 10.1039/D1CP03410D

To understand the hypsochromic effect observed in crystal, a series of DFT and DFT:MM calculations has been made, for the complex in both its singlet (ground state) and triplet (excited state) configurations, in vacuum and embedded in a model of crystal. The structure was thus optimized at MN15/Def2SVP level of theory for the isolated complex and MN15/Def2SVP:UFF levels of theory for the complex in crystal (see computational detail), both for the singlet ground state (S) and triplet excited state (T). Using these models, we first have computed the λ_{max} of the emission associated to the triplet to singlet vertical luminescence transition. This value, noted $\Delta E_{T\rightarrow S}$, is computed as the difference between the energy of the optimized triplet structure ($E_{T(T)}$) and of the singlet structure ($E_{S(T)}$), with the triplet geometry ($\Delta E_{T\rightarrow S} = E_{T(T)} - E_{S(T)}$) since the emission is considered to be associated with a vertical transition. Values obtained for the single complex and for the crystal model are reported in Table 4 and compared to the experimental results obtained in powder and in the crystal. The table compares both the $\Delta E_{T\rightarrow S(T)}$ and corresponding λ_{max} values:

Compared to experimental data from powder, the $\Delta E_{T\rightarrow S}$ given by the single complex model is overestimated by 0.09eV. Comparing crystal model and experimental results also shows an overestimation of 0.24eV. However, calculations account for the hypsochromic effect with an overestimated decrease of the λ_{max} of -57 nm (561 nm to 504 nm), to be compared to the 27 nm obtained experimentally. We thus consider that our model is able to reproduce the experimental findings and is therefore suitable to investigate the actual nature of the influence of the crystal. This influence of the surrounding can be split into two main components: a steric effect, that can modify the complex structure upon crystallization and a polarization effect, due to the charges of surrounding molecules. Both have been evaluated using the DFT:MM model.

The mechanical influence was first evaluated by comparing the geometries of the triplet structures (excited states giving rise to emission) optimized in vacuum and in the crystal. A structure alignment shows very similar geometries, with a computed RMSD of only 0.24 Å. This limited influence of the crystal on the structure of the complex is consistent with quite a "rigid" complex structure. One can specifically remark that, when putting the complex out of the crystal, the four Ir-N distances do not vary while the two Ir-C bonds marginally shrink from 2.02 Å to 2.00 Å. Since the crystalline environment keeps the geometry of the complex essentially unchanged compared to the one of the complex alone, one can thus deduce that the hypsochromic effect observed might be rather due to the polarization effects of the crystalline structure.

Table 4: Energy difference and corresponding λ_{max} of emission between the triplet and singlet states for the complex alone or in crystal. Experimental values also provided for comparison purpose.

	$\Delta E_{T\rightarrow S(T)}$	λ_{max}
Single complex model	2.21 eV	561 nm
Crystal model	2.46 eV	504 nm
Amorphous powder (exp)	2.12 eV	585 nm
Crystals (exp)	2.22 eV	558 nm

To evaluate this effect, the $\Delta E_{T\rightarrow S}$ for the complex in its crystal geometry, but without the surrounding charges has been compared to the one obtained in the complete model. A value of 2.19 eV was found, very similar (even smaller) to the value found in vacuum. This thus confirms that the observed hypsochromism is due to the polarization effects of the crystalline environment.

In order to understand this polarizing effect of the surroundings and especially discriminate between long- and short-range effects, the $\Delta E_{T\rightarrow S}$ has been computed for a smaller crystal model in which only the first neighbours of the complex (other complexes and counterions, all at the MM level) were kept. The value found, 2.48 eV, is essentially the same as in the "big" model, showing an exclusively short-range effect. Finally, the calculation of $\Delta E_{T\rightarrow S(T)}$ was done for a complex in interaction with either the nearest equivalent complex or the nearest PF_6^- counterion. The presence of the nearest complex only (at the MM level) yields to a $\Delta E_{T\rightarrow S}$ of 2.14 eV, very similar to the result in vacuum, thus discarding a strong complex/complex interaction. On the opposite, the presence of the nearest counterion only, yields to a $\Delta E_{T\rightarrow S(T)}$ of 2.41 eV, almost unchanged compared to the largest crystal model. This result unambiguously proves that the hypsochromic effect is due to the presence of a negatively charged counterion located near each complex in the crystal. Interestingly, even the replacement of PF_6^- by a negative point charge at the position of the P atom yields to an hypsochromic shift of 2.43 eV. This PF_6^- anion is positioned at a peculiar place and interacts strongly through hydrogen bonding with H20 of the dmp ligand (vide supra) and the negative charge of the anion destabilizes the excited state. Indeed, the dipole moment in this complex is roughly oriented from the electron rich iridium toward the electron poor dmp ligand in the ground state[85,86]. In the excited state the electron density is inverted, and so is the dipole moment. Due to its specific position, the PF_6 anion will more "perturbate" the excited state than the ground state, thus leading to an increase of the $\Delta E_{T\rightarrow S}$ and a hypsochromic shift of the emission in crystals. To illustrate this hypothesis, we have compared the dipole moments from DFT calculations, for the complex in its singlet and triplet states, in presence or absence of a negative point charge of -e at the position of the P atom, all using the geometry from the crystal. Because the complex is positively charged, its dipole is gauge-dependent (depends on position

Figure 11. Representation of the dipole of the complex at the origin without counterion (orange: singlet, green: triplet) or in presence of a negative charge at the position of the P atom of the counterion (red: singlet, blue: triplet)

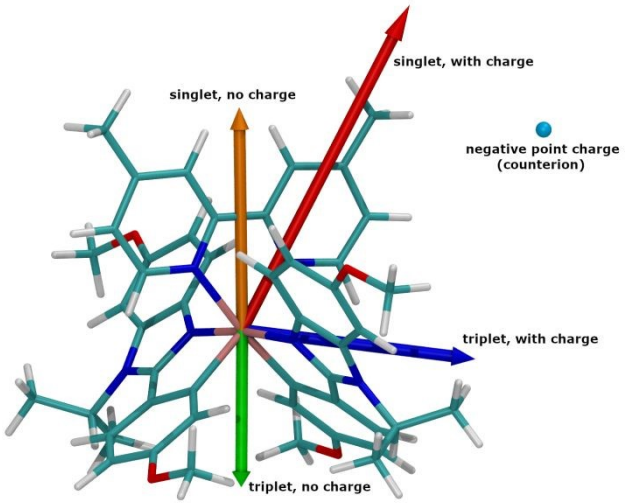

and orientation). A special care has thus been taken to carry calculations on the same structure (same geometry, same orientation) with or without the charge, in the triplet and singlet states.

Figure 11 represents the dipole as an arrow starting from the origin. The scale is 1 Debye for one Å. The orange arrow is for the complex in its singlet state, without charge, green when in triplet without charge. In the presence of the charge, the dipole for the singlet state is shown in red and the one for the triplet state is in blue. As stated, the singlet and triplet structures have opposite dipoles when complex is isolated, both along the C2 rotation axis. In the presence of the charge (blue sphere), both the dipoles (red: singlet, blue: triplet) are modified and now partially point towards the negative charge. As shown by **Figure 11**, the triplet dipole is more affected than the singlet one, consistently with a more perturbed electron structure and a $\Delta E_{T\rightarrow S}$ value increase in the presence of the negative charge, i.e., in the crystal structure.

Figure 11 represents the dipole as an arrow starting from the origin. The scale is 1 Debye for one Å. The orange arrow is for the complex in its singlet state, without charge, green when in triplet without charge. In the presence of the charge, the dipole for the singlet state is shown in red and the one for the triplet state is in blue. As stated, the singlet and triplet structures have opposite dipoles when complex is isolated, both along the C2 rotation axis. In the presence of the charge (blue sphere), both the dipoles (red: singlet, blue: triplet) are modified and now partially point towards the negative charge. As shown by **Figure 11**, the triplet dipole is more affected than the singlet one, consistently with a more perturbed electron structure and a $\Delta E_{T\rightarrow S}$ value increase in the presence of the negative charge, i.e., in the crystal structure.

Conclusions

In summary, we have reported the synthesis and the characterization of a new cationic iridium(III) complex featuring two 1-(*p*-methoxyphenyl)-5-methoxybenzimidazole cyclometallating ligands and a dimethylbipyridine ancillary ligand. The single crystal structure and the powder X-ray diffraction have been presented. The photophysical studies of the complex point out a strong change in the emission wavelength of the complex between CH_2Cl_2 solution and the amorphous powder in comparison with crystals, with a hypsochromic shift of the order 800 cm^{-1}, whereas (i) the majority of cationic iridium complexes display a bathochromic shift from solution to neat solid, and (ii) the few observed hypsochromic shifts are on average 600 cm^{-1}. The study of the single crystal XRD and in particular the packing of the molecules in the lattice suggest that the observed shift can be explained by the destabilizing effect of the neighbouring counterion in the crystal on the dipole moment of the complexes. This result is supported by the calculation that fits very well the experimental data. These results highlight how packing can perturb the photophysical properties of the molecules, even in the absence of particularly short interactions.

Conflicts of interest

There are no conflicts to declare.

Acknowledgements

The authors thank the CNRS and Université de Grenoble Alpes for their support. This work benefited from state aid managed by the National Research Agency under the “Investments for the future” and of the "Investissements d’avenir" program bearing the reference ANR-15-IDEX-02”. E. Martinez-Vollbert benefits of a CONACYT program (707986). This work was partially supported by CBH-EUR-GS (ANR-17-EURE-0003). The NanoBio ICMG (UAR 2607) is acknowledged for providing facilities for mass spectrometry (A. Durand, L. Fort and R. Gueret), elemental analyses (M. Fayolle) and single crystal X-ray diffraction (N. Altounian).

The solid-state emission measurements have been performed in the “Laboratoire de Chimie” (UMR-5182) at the “Ecole Nationnale Supérieure de Lyon” (ENSL).

Notes

§ The F2 atom presents disorder and it is defined with 2 positions F2A and F2B in cif file.

§§The quenching rate constants are extracted from $\frac{\Phi_0}{\Phi} = 1 + \tau_0 k_Q [O_2]$ with Φ_0 PLQY deaerated, Φ PLQY under air, τ_0 deaerated lifetime and $[O_2]$ the concentration of molecular oxygen in the solvent under normal pressure at r.t..

References

1 W. C. H. Choy, W. K. Chan and Y. Yuan, *Adv. Mater.*, 2014, **26**, 5368–5399.
2 K. K.-W. Lo, *Acc. Chem. Res.*, 2015, **48**, 2985–2995.
3 Y. J. Yuan, Z. T. Yu, D. Q. Chen and Z. G. Zou, *Chem. Soc. Rev.*, 2017, **46**, 603–631.

4 C. K. Prier, D. a Rankic and D. W. C. MacMillan, *Chem. Rev.*, 2013, **113**, 5322–5363.

5 J. H. Shon and T. S. Teets, *ACS Energy Lett.*, 2019, **4**, 558–566.

6 Q. Zhao, L. Li, F. Li, M. Yu, Z. Liu, T. Yi and C. Huang, *Chem. Commun.*, 2008, **3**, 685–687.

7 L. Flamigni, A. Barbieri, C. Sabatini, B. Ventura and F. Barigelletti, in *Photochemistry and Photophysics of Coordination Compounds II*, 2007, pp. 143–203.

8 K. P. S. Zanoni, R. L. Coppo, R. C. Amaral and N. Y. Murakami Iha, *Dalt. Trans.*, 2015, **44**, 14559–14573.

9 P. A. Scattergood, A. M. Ranieri, L. Charalambou, A. Comia, D. A. W. Ross, C. R. Rice, S. J. O. Hardman, J.-L. Heully, I. M. Dixon, M. Massi, F. Alary and P. I. P. Elliott, *Inorg. Chem.*, 2020, **59**, 1785–180.

10 X. Yan, H. Wang, C. E. Hauke, T. R. Cook, M. Wang, M. L. Saha, Z. Zhou, M. Zhang, X. Li, F. Huang and P. J. Stang, *J. Am. Chem. Soc.*, 2015, **137**, 15276–15286.

11 T. Sajoto, P. I. Djurovich, A. B. Tamayo, J. Oxgaard, W. A. Goddard and M. E. Thompson, *J. Am. Chem. Soc.*, 2009, **131**, 9813–9822.

12 Y. Kawamura, K. Goushi, J. Brooks, J. J. Brown, H. Sasabe and C. Adachi, *Appl. Phys. Lett.*, 2005, **86**, 71104.

13 Y. Kawamura, H. Sasabe and C. Adachi, *Jpn. J. Appl. Phys.*, 2004, **43**, 7729–7730.

14 N. Komiya, M. Okada, K. Fukumoto, D. Jomori and T. Naota, *J. Am. Chem. Soc.*, 2011, **133**, 6493–6496.

15 X. Wang, S. Wang, F. Pan, L. He and L. Duan, *Inorg. Chem.*, 2019, **58**, 12132–12145.

16 E. C. Constable, C. E. Housecroft, G. E. Schneider, J. A. Zampese, H. J. Bolink, A. Pertegás and C. Roldan-Carmona, *Dalt. Trans.*, 2014, **43**, 4653–4667.

17 A. F. Henwood, A. K. Pal, D. B. Cordes, A. M. Z. Slawin, T. W. Rees, C. Momblona, A. Babaei, A. Pertegás, E. Ortí, H. J. Bolink, E. Baranoff and E. Zysman-Colman, *J. Mater. Chem. C*, 2017, **5**, 9638–9650.

18 G. Rajendra Kumar and P. Thilagar, *Inorg. Chem.*, 2016, **55**, 12220–12229.

19 N. Komiya, M. Okada, K. Fukumoto, K. Kaneta, A. Yoshida and T. Naota, *Chem. Eur. J.*, 2013, **19**, 4798–4811.

20 H. J. Bolink, E. Coronado, R. D. Costa, N. Lardiés and E. Ortí, *Inorg. Chem.*, 2008, **47**, 9149–9151.

21 V. Sathish, A. Ramdass, P. Thanasekaran, K. L. Lu and S. Rajagopal, *J. Photochem. Photobiol. C Photochem. Rev.*, 2015, **23**, 25–44.

22 H. Wu, T. Yang, Q. Zhao, J. Zhou, C. Li and F. Li, *Dalt. Trans.*, 2011, **40**, 1969–1976.

23 J. Han, K. Tang and S. Cheng, *Inorg. Chem. Front.*, 2020, **7**, 786–794.

24 H.-C. Su, H.-F. Chen, F.-C. Fang, C.-C. Liu, C.-C. Wu, K.-T. Wong, Y.-H. Liu and S.-M. Peng, *J. Am. Chem. Soc.*, 2008, **130**, 3413–3419.

25 L. He, L. Duan, J. Qiao, G. Dong, L. Wang and Y. Qiu, *Chem. Mater.*, 2010, **22**, 3535–3542.

26 L. He, D. Ma, L. Duan, Y. Wei, J. Qiao, D. Zhang, G. Dong, L. Wang and Y. Qiu, *Inorg. Chem.*, 2012, **51**, 4502–4510.

27 S. Evariste, M. Sandroni, T. W. Rees, C. Roldán-Carmona, L. Gil-Escrig, H. J. Bolink, E. Baranoff and E. Zysman-Colman, *J. Mater. Chem. C*, 2014, **2**, 5793.

28 K. P. S. Zanoni, M. S. Sanematsu and N. Y. Murakami Iha, *Inorg. Chem. Commun.*, 2014, **43**, 162–164.

29 G. G. Shan, H. Bin Li, Z. C. Mu, D. X. Zhu, Z. M. Su and Y. Liao, *J. Organomet. Chem.*, 2012, **702**, 27–35.

30 Y. Lan, G. Li, Z. Wang, Y. He, Y. Liu and L. He, *Dye. Pigment.*, 2017, **144**, 158–167.

31 K. J. Suhr, L. D. Bastatas, Y. Shen, L. A. Mitchell, G. A. Frazier, D. W. Taylor, J. D. Slinker and B. J. Holliday, *Dalt. Trans.*, 2016, **45**, 17807–17823.

32 E. Matteucci, A. Baschieri, A. Mazzanti, L. Sambri, J. Ávila, A. Pertegás, H. J. Bolink, F. Monti, E. Leoni and N. Armaroli, *Inorg. Chem.*, 2017, **56**, 10584–10595.

33 C. Hierlinger, D. B. Cordes, A. M. Z. Slawin, D. Jacquemin, V. Guerchais and E. Zysman-Colman, *Dalt. Trans.*, 2018, **47**, 10569–10577.

34 L. P. Li, S. Y. Yao, Y. L. Ou, L. Q. Wei and B. H. Ye, *Organometallics*, 2017, **36**, 3257–3265.

35 J. D. Slinker, A. A. Gorodetsky, M. S. Lowry, J. Wang, S. Parker, R. Rohl, S. Bernhard and G. G. Malliaras, *J. Am. Chem. Soc.*, 2004, **126**, 2763–2767.

36 H. Cao, H. Sun, G. Shan, Y. Wu, Z. Su and Y. Liao, *J. Mater. Chem. C*, 2015, 2341–2349.

37 K. J. Suhr, L. D. Bastatas, Y. Shen, L. A. Mitchell, B. J. Holliday and J. D. Slinker, *ACS Appl. Mater. Interfaces*, 2016, **8**, 8888–8892.

38 K. Traskovskis, V. Kokars, S. Belyakov, N. Lesina, I. Mihailovs and A. Vembris, *Inorg. Chem.*, 2019, **58**, 4214–4222.

39 G. G. Shan, H. Bin Li, H. T. Cao, D. X. Zhu, P. Li, Z. M. Su and Y. Liao, *Chem. Commun.*, 2012, **48**, 2000–2002.

40 G. Shan, H.-B. Li, D.-X. Zhu, Z.-M. Su and Y. Liao, *J. Mater. Chem.*, 2012, **22**, 12736–12744.

41 Z. Chi, X. Zhang, B. Xu, X. Zhou, C. Ma, Y. Zhang, S. Liu and J. Xu, *Chem. Soc. Rev.*, 2012, **41**, 3878–3896.

42 C. E. Housecroft and E. C. Constable, *Coord. Chem. Rev.*, 2017, **350**, 155–177.

43 L. He, Y. Lan, D. Ma, X. Song and L. Duan, *J. Mater. Chem. C*, 2018, **6**, 1509–1520.

44 C. D. Ertl, C. Momblona, A. Pertegás, J. M. Junquera-Hernández, M. G. La-Placa, A. Prescimone, E. Ortí, C. E. Housecroft, E. C. Constable and H. J. Bolink, *J. Am. Chem. Soc.*, 2017, **139**, 3237–3248.

45 A. F. Henwood and E. Zysman-Colman, *Top. Curr. Chem.*, , DOI:10.1007/s41061-016-0036-0.

46 R. D. Costa, E. Ortí, H. J. Bolink, S. Graber, S. Schaffner, M. Neuburger, C. E. Housecroft and E. C. Constable, *Adv. Funct. Mater.*, 2009, **19**, 3456–3463.

47 Y. Jiao, M. Li, N. Wang, T. Lu, L. Zhou, Y. Huang, Z. Lu, D. Luo and X. Pu, *J. Mater. Chem. C*, 2016, **4**, 4269–4277.

48 T. Yu, F. Yang, X. Chen, W. Su and Y. Zhao, *New J. Chem.*, 2017, **41**, 2046–2054.

49 H.-T. T. Mao, C.-X. X. Zang, G.-G. G. Shan, H.-Z. Z. Sun, W.-F. F. Xie and Z.-M. M. Su, *Inorg. Chem.*, 2017, **56**, 9979–9987.

50 J. E. Yarnell, P. De La Torre and F. N. Castellano, *Eur. J. Inorg. Chem.*, 2017, 1–9.

51 J.-H. Zhao, Y.-X. Hu, Y. Dong, X. Xia, H.-J. Chi, G.-Y. Xiao, X. Li and D.-Y. Zhang, *New J. Chem.*, 2017, **41**, 1973–1979.

52 J. F. Lemonnier, L. Guénée, C. Beuchat, T. A. Wesolowski, P. Mukherjee, D. H. Waldeck, K. A. Gogick, S. Petoud and C. Piguet, *J. Am. Chem. Soc.*, 2011, **133**, 16219–16234.

53 N. M. Shavaleev, S. V. Eliseeva, R. Scopelliti and J. C. G. Bünzli, *Chem. Eur. J.*, 2009, **15**, 10790–10802.

54 S. Sprouse, K. A. King, P. J. Spellane and R. J. Watts, *J. Am. Chem. Soc.*, 1984, **106**, 6647–6653.

55 D. J. Frisch, M. J.; Trucks, G. W.; Schlegel, H. B.; Scuseria, G. E.; Robb, M. A.; Cheeseman, J. R.; Scalmani, G.; Barone, V.; Petersson, G. A.; Nakatsuji, H.; Li, X.; Caricato, M.; Marenich, A. V.; Bloino, J.; Janesko, B. G.; Gomperts, R.; Mennucci, B.; Hratch, 2016.

56 S. Dapprich, I. Komáromi, K. S. Byun, K. Morokuma and M. J. Frisch, *J. Mol. Struct. THEOCHEM*, 1999, **461–462**, 1–21.

57 H. S. Yu, X. He, S. L. Li and D. G. Truhlar, *Chem. Sci.*, 2016, **7**, 5032–5051.

58 F. Weigend and R. Ahlrichs, *Phys. Chem. Chem. Phys.*, 2005, **7**, 3297–3305.

59 F. Weigend, *Phys. Chem. Chem. Phys.*, 2006, **8**, 1057–1065.

60 A. K. Rappe, C. J. Casewit, K. S. Colwell, W. A. Goddard and W. M. Skiff, *J. Am. Chem. Soc.*, 1992, **114**, 10024–10035.

61 C. F. Macrae, I. Sovago, S. J. Cottrell, P. T. A. Galek, P. Mccabe, E. Pidcock, M. Platings, G. P. Shields, J. S. Stevens, M. Towler and P. A. Wood, *J. Appl. Cryst*, 2020, **53**, 226–235.

62 D. A. Case, K. Belfon, I. Y. Ben-Shalom, S. R. Brozell, S. D. Cerutti, T. Cheatham, E., V. W. D. Cruzeiro III, A. T. Darden, R. E. Duke, G. Giambasu, M. K. Gilson, H. Gohlke, A. W. Goetz, R. Harris, S. Izadi, S. A. Izmailov, K. Kasavajhala, A. Kovalenko, R. Krasny, T. Kurtzman, T. S. Lee, S. Le Grand, P. Li, C. Lin, J. Liu, T. Luchko, R. Luo, V. Man, K. M. Merz, Y. Miao, O. Mikhailovskii, G. Monard, H. Nguyen, A. Onufriev, F. Pan, S. Pantano, R. Qi, D. R. Roe, A. Roitberg, C. Sagui, S. Schott-Verdugo, J. Shen, C. L. Simmerling, N. R. Skrynnikov, J. Smith, J. Swails, R. C. Walker, J. Wang, L. Wilson, R. M. Wolf, X. Wu, Y. Xiong, Y. Xue, D. M. York and P. A. Kollman, 2020.

63 R. Bjornsson and M. Bühl, *J. Chem. Theory Comput.*, 2012, **8**, 498–508.

64 L. E. Chirlian and M. M. Francl, *J. Comput. Chem.*, 1987, **8**, 894–905.

65 C. M. Breneman and K. B. Wiberg, *J. Comput. Chem.*, 1990, **11**, 361–373.

66 U. C. Singh and P. A. Kollman, *J. Comput. Chem.*, 1984, **5**, 129–145.

67 S. I. Bezzubov, Y. M. Kiselev, A. V. Churakov, S. A. Kozyukhin, A. A. Sadovnikov, V. A. Grinberg, V. V. Emets and V. D. Doljenko, *Eur. J. Inorg. Chem.*, 2016, **2016**, 347–354.

68 E. Baranoff, H. J. Bolink, E. C. Constable, M. Delgado, D. Häussinger, C. E. Housecroft, M. K. Nazeeruddin, M. Neuburger, E. Ortí, G. E. Schneider, D. Tordera, R. M. Walliser and J. A. Zampese, *Dalt. Trans.*, 2013, **42**, 1073–1087.

69 M. Martínez-Alonso, J. Cerdá, C. Momblona, A. Pertegás, J. Junquera-Hernández, A. Heras, A. M. Rodríguez, G. Espino, H. Bolink and E. Ortí, *Inorg. Chem.*, 2017, **56**, 10298–10310.

70 K. A. Phillips, T. M. Stonelake, K. Chen, Y. Hou, J. Zhao, S. J. Coles, P. N. Horton, S. J. Keane, E. C. Stokes, I. A. Fallis, A. J. Hallett, S. P. O'Kell, J. M. Beames and S. J. A. Pope, *Chem. Eur. J.*, 2018, **24**, 8577–8588.

71 D. G. Congrave, Y. ting Hsu, A. S. Batsanov, A. Beeby and M. R. Bryce, *Organometallics*, 2017, **36**, 981–993.

72 T. Steiner, *Angew. Chemie - Int. Ed.*, 2002, **41**, 48–76.

73 D. Avobenzone, G. Zhang, J. Lu, M. Sabat and C. L. Fraser, *J. Am. Chem. Soc.*, 2010, **132**, 2160–2162.

74 T. F. Mastropietro, Y. J. Yadav, E. I. Szerb, A. M. Talarico, M. Ghedini and A. Crispini, *Dalt. Trans.*, 2012, **41**, 8899–8907.

75 Bingjia, H. Xu, Y. Jiajun Mu, Q. Zhu, S. Wu, Y. Wang, Y. Zhang, C. Jin, C. Lo, Z. Chi, A. Lien, S. Liua and J. Xu, *Chem. Sci.*, 2015, 3236–3241.

76 Y. You, H. S. Huh, K. S. Kim, S. W. Lee, D. Kim and S. Y. Park, *Chem. Commun.*, 2008, 3998–4000.

77 K. Hasan, A. K. Bansal, I. D. W. Samuel, C. Roldán-Carmona, H. J. Bolink and E. Zysman-Colman, *Sci. Rep.*, 2015, **5**, 1–16.

78 A. J. Lees, *Comments Inorg. Chem. A J. Crit. Discuss. Curr. Lit.*, 1995, **17**, 319–346.

79 D. Tran, J. L. Bourassa and P. C. Ford, *Inorg. Chem.*, 1997, **36**, 439–442.

80 S. Nayeri, S. Jamali, A. Jamjah and H. Samouei, *Inorg. Chem.*, 2019, **58**, 12122–12131.

81 M. A. Halcrow, *Chem. Soc. Rev.*, 2013, **42**, 1784–1795.

82 F. Würthner, T. E. Kaiser and C. R. Saha-Möller, *Angew. Chemie - Int. Ed.*, 2011, **50**, 3376–3410.

83 A. Mishra, R. K. Behera, P. K. Behera, B. K. Mishra and G. B. Behera, *Chem. Rev.*, 2000, **100**, 1973–2011.

84 E. Quartapelle Procopio, M. Mauro, M. Panigati, D. Donghi, P. Mercandelli, A. Sironi, G. D'Alfonso and L. De Cola, *J. Am. Chem. Soc.*, 2010, **132**, 14397–14399.

85 J. M. Fernaíndez-Hernaíndez, C. H. Yang, J. I. Beltraín, V. Lemaur, F. Polo, R. Fröhlich, J. Cornil and L. De Cola, *J. Am. Chem. Soc.*, 2011, **133**, 10543–10558.

86 A. Valore, E. Cariati, C. Dragonetti, S. Righetto, D. Roberto, R. Ugo, F. De Angelis, S. Fantacci, A. Sgamellotti, A. Macchioni and D. Zuccaccia, *Chem. Eur. J.*, 2010, **16**, 4814–4825.